Proceedings of *RAGtime 20–22, 15–19 Oct., 16–20 Sept., 19–23 Oct., 2018/2019/2020, Opava, Czech Republic*
Z. Stuchlík, G. Török and V. Karas, editors, Silesian University in Opava, 2020, pp. 383–396

Understanding the iron Kα line emissivity profile with GR radiative transfer code

Wenda Zhang[1,a], Michal Dovčiak[1], Michal Bursa[1], Jiří Svoboda[1] and Vladimír Karas[1]

[1] Astronomical Institute, Czech Academy of Sciences, Boční II, CZ-141 31 Prague, Czech Republic
[a] zhang@asu.cas.cz

ABSTRACT
One of the most promising methods to measure the spin of an accreting black hole is fitting the broad iron Kα line in the X-ray spectrum. The line profile also depends on the geometry of the hard X-ray emitting corona. To put constraints on the black hole spin and corona geometry, it is essential to understand how do they affect the iron Kα line emissivity profile, i.e., the local emissivity of the iron Kα emission as a function of the radius on the accretion disc. In this work, we present calculations of the illumination and the iron Kα emissivity profiles performed with the GR radiative transfer code Monk that employs the Monte Carlo method. In most previous studies the distinction between the illumination and emissivity profiles was not clearly made. For AGN discs, the emissivity profile has a similar shape with the illumination profile, but in the innermost region the former is steeper than the latter; whereas for accretion discs in black hole X-ray binaries, the distinction between the two profiles is more dramatic. We find out that the different behavior between AGN and black hole X-ray binary discs is due to the different energy spectra of the illuminating radiation. This suggests that the emissivity profile of the iron Kα line cannot be determined by black hole spin and corona geometry alone and the energy spectrum of the illuminating radiation has to be taken into account. We also study the dependence of the emissivity profile on the geometry of the corona.

1 INTRODUCTION

X-ray spectra of Active Galactic Nuclei (AGNs) and X-ray binaries (XRBs) exhibit signatures of X-ray reflection, including iron K fluorescent lines and the Compton hump (see the review of Miller, 2007). It is generally believed that they are due to the hard X-ray radiation of the corona illuminating the underlying accretion disc (see Fabian and Ross, 2010 and references therein). The iron line is intrinsically narrow, but the observer at infinity sees broad and asymmetric line profile, due to the gravitational redshift by the strong gravitational field of the black hole and Doppler broadening of the accretion disc (Fabian et al., 1989; Laor, 1991). The shape of the broad iron line depends on the black hole spin, and thus fitting the iron line profile is one of the most promising methods of measuring the spin

of accreting black holes (e.g., Miller et al., 2009). For Sgr A*, constraints on the black hole spin can also be put by analyzing the polarization and/or variability of its emission (e.g., Eckart et al., 2006; Trippe et al., 2007; Shcherbakov et al., 2012; Karssen et al., 2017).

To put a constraint on the black hole spin it is important to know the radial emissivity profile of the iron fluorescent lines and the effect of altering black hole spin on the emissivity profile. Martocchia et al. (2000) and Miniutti et al. (2003) studied the emissivity profile of an accretion disc illuminated by a point-like source above the disc and found the profile to be a three-segment broken power-law. Dovciak et al. (2014) investigated in detail the dependence of the emissivity profile on the black hole spin and corona height assuming the lamp-post geometry. Analysis of the emissivity profile of accretion discs irradiated by extended coronae was performed by Wilkins and Fabian (2012) and Gonzalez et al. (2017).

In most of the previous studies, the authors made no clear distinction between the illumination profile (the total energy of illuminating radiation per unit time per unit area) and the emissivity profile of a particular radiative process (the number of photons emitted per unit time per unit area). Also, simple assumptions were made for the spectrum of the illuminating radiation. For example, when calculating the iron Kα emissivity profile the spectrum was usually assumed to have power-law shape in the energy band most relevant for iron K fluorescent lines. Unlike the illumination profile, the emissivity profile also depends on the specific radiative process and is thus sensitive to the local energy spectrum of the illuminating radiation. In this work, we present the illumination and iron Kα emissivity profiles obtained with the general relativistic (GR) Monte Carlo radiative transfer code Monk (Zhang et al., 2019). Thanks to its Monte Carlo nature we are able to calculate not only the flux but also the spectrum of the illuminating radiation as measured in the rest frame of the disc fluid for accretion discs illuminated by extended coronae. As a result, we are able to calculate both the illumination and the emissivity profiles.

2 PROCEDURE

2.1 Calculating the illumination and emissivity profiles

We calculate the illumination and emissivity profiles of a thin Keplerian disc illuminated by an optically-thin extended corona. The thin disc extends down to the innermost circular stable orbit (ISCO). We assume that the thin disc follows Novikov-Thorne temperature profile and there is zero torque at the inner boundary. Following the "superphoton scheme" (Dolence et al., 2009), we sample seed superphotons from the thin disc and propagate the superphotons along null geodesics in the Kerr spacetime (for details see Zhang et al. 2019, submitted). Each superphoton is characterised by its energy at infinity E_∞, weight w, initial position x^μ_0, and initial wave vector k^μ_0. Its weight w has the physical meaning of superphoton generation rate per unit time in a distant observer's frame. If the superphoton is traveling inside the extended corona, we set the step of raytracing to be much less than the scattering mean free path and for each step, we evaluate the Compton scattering optical depth. If the superphoton is scattered, we sample the energy and momentum of the scattered superphoton assuming Klein-Nishina differential cross-section. Finally, we collect superphotons that arrive at the thin disc. For each superphoton, we have the following information: E_∞, w, and its position x^μ and wave-vector k^μ while hitting the disc.

We divide the accretion disc into several radial bins, from ISCO to 100 GM/c^2. The proper area of the i-th bin is

$$\mathcal{S}_i = \int_{r_i}^{r_{i+1}} \frac{2\pi\rho\gamma}{\sqrt{\Delta}} \sqrt{r^2 + a^2 + \frac{2a^2 r}{\rho^2}} \mathrm{d}r, \tag{1}$$

where $\rho^2 \equiv r^2 + a^2\cos^2\theta$, and $\Delta \equiv r^2 - 2r + a^2$, γ is the Lorentzian factor of the disc fluid as measured by a stationary observer, and r_i, r_{i+1} are the lower and upper boundaries of the i-th radial bin. To translate the time from a distant observer's frame to the local frame, we calculate $u^t \equiv dt/d\tau$:

$$u^t = \frac{1}{\sqrt{1 - 2/r + 4\Omega a/r - \Omega^2(r^2 + a^2 + 2a^2/r)}}, \tag{2}$$

where Ω is the angular velocity of the disc fluid. In the i-th radial bin, the flux of the illuminating radiation in the unit of energy per unit time per unit area as measured by the disc fluid is

$$\epsilon_i = \frac{\sum w E_{\rm disc} u_i^t}{\mathcal{S}_i}, \tag{3}$$

where the sum is over all Comptonised photons that strike the thin disc between r_i and r_{i+1}, and $E_{\rm disc}$ is the photon energy measured by the disc fluid. Denoting the four-velocity of the disc fluid U^μ, we have $E_{\rm disc} = -k^\mu U_\mu E_\infty$.

The probability for a hard X-ray photon to produce an iron Kα photon while striking the neutral disc (e.g., George and Fabian, 1991):

$$P(E) \propto \frac{n_{\rm Fe}\sigma_{\rm Fe}(E)}{\sum n_j \sigma_{\rm j,abs}(E) + n_e \sigma_{\rm sca}(E)}, \tag{4}$$

if the energy of the hard X-ray photon is above neutral iron K edge $E_K \sim 7.12$ keV, where $n_{\rm Fe}$ is the number density of neutral iron, n_j is the number density of the j-th ion species, n_e is the number density of electron, σ_{Fe} is the photon-ionisation cross section of neutral iron, $\sigma_{j,abs}$ is the photon-ionisation cross section of the j-th ion species, and $\sigma_{\rm sca}$ is the Compton scattering cross section. As $\sigma_{Fe}, \sigma_{\rm sca} \propto E^{-3}$ while $\sigma_{\rm sca}$ is varying slowly with energy, $P(E)$ decreases with energy rapidly and the photons with energy just above the iron K edge are most essential for the production of iron Kα photons (George and Fabian, 1991).

In the i-th radial bin, the emissivity of iron Kα photon, i.e., the number of iron Kα photons produced per unit area per unit time in the local frame is

$$\varepsilon_i = \frac{\sum w P(E_{\rm disc}) u_i^t}{\mathcal{S}_i}. \tag{5}$$

where the sum is over all superphotons with $r_i \le r \le r_{i+1}$ and $E_{\rm disc} \ge E_K$.

In this paper we assume that the elements in the disc atmosphere are neutral and have solar abundance (Grevesse and Sauval, 1998). The photon ionisation cross sections are calculated with analytical formula by Verner and Yakovlev (1995). For Compton scattering we assume Klein-Nishina scattering cross section.

2.2 Relation between the illumination and emissivity profiles

Let us assume that the spectra of the illuminating radiation at different radii on the disc is different only by different normalisations and redshift (which is the case for an isotropic, lamp-post corona). In this case, we can write the count spectrum of the illuminating radiation as observed by the disc fluid located at radius r as

$$N(E, r) = F(r) f\left(\frac{E}{g(r)}\right) \frac{1}{g(r)}, \tag{6}$$

where $g(r)$ is the dependence of redshift factor $g \equiv E_{\rm disc}/E_{\infty}$ on radius. Then

$$\epsilon(r) = \int_0^{\infty} EN(E, r) dE = F(r) g(r), \tag{7}$$

whatever shape the spectrum has. The iron Kα emissivity profile

$$\varepsilon(r) = \int_{E_K}^{\infty} N(E, r) P(E) dE = \frac{F(r)}{g(r)} \int_{E_K}^{\infty} P(E) f\left(\frac{E}{g(r)}\right) {\rm d}E. \tag{8}$$

For Comptonised spectrum the high energy spectrum can usually be described by a cut-off power-law function. In this case $f(E) = E^{-\Gamma} e^{-E/E_{\rm cut}}$ for $E \geq E_0$, where Γ is the photon index, $E_{\rm cut}$ is the high-energy cut-off energy, and E_0 is the energy of the low-energy cut-off. If $E_0 \leq E_K/max(g(r))$, then

$$\varepsilon(r) = F(r) g^{\Gamma-1}(r) \int_{E_K}^{\infty} P(E) E^{-\Gamma} e^{-E/g(r)E_{\rm cut}} {\rm d}E. \tag{9}$$

For the iron Kα emissivity profile, as $P(E)$ decrease rapidly with energy, the integral is not sensitive to $g(r)$, therefore

$$\varepsilon(r) \propto F(r) g^{\Gamma-1}(r), \tag{10}$$

and

$$\frac{\varepsilon(r)}{\epsilon(r)} \propto g^{\Gamma-2}(r). \tag{11}$$

We can see that whether the emissivity profile is steeper than the illumination profile depends on the value of Γ and the slope of $g(r)$.

3 RESULTS

3.1 Stationary spherical corona in AGNs

In this section, we present the illumination and emissivity profiles of accretion discs illuminated by a spherical corona above the disc. We assume a maximally rotating black hole ($a = 0.998$), to investigate the profiles around a rotating black hole. The effect of the black hole spin will be carried out in a future work. The black hole has a mass of 10^7 $M_{\odot}$ and is

accreting with a mass accretion rate of 4.32×10^{23} g s^{-1}. Assuming the radiative efficiency to be 0.354 for a $a = 0.998$ black hole, the bolometric luminosity is expected to be $\sim 10\%$ the Eddington luminosity, more or less the median Eddington rate of X-ray selected AGNs (Lusso et al., 2012). The spherical corona is stationary, i.e., the fluid has the same angular velocity with a zero angular momentum observer. Although the assumption of a stationary corona is somewhat unphysical, it has been taken in many previous studies where the observations were successfully described. Since in this work we are mainly investigating the effect of the corona geometry on the illumination and emissivity profiles, we still take this assumption, but calculations with more realistic assumptions of the coronae will be carried out in a future work. The temperature of the corona is 100 keV, and the Thomson optical depth of the corona $\tau_{\rm T} \equiv \sigma_T n_e R_c = 0.2$, where $\sigma_{\rm T}$ is the Thomson scattering cross section, and R_c is the radius of the corona.

3.1.1 Dependence on corona size

In Fig. 1 we present the illumination and emissivity profiles for spherical coronae of different sizes. The center of the corona is located on the black hole rotation axis, 10 GM/c^2 above the equatorial plane. For all corona sizes the emissivity profile seems to be quite steep at the innermost region of the accretion disc (below $\sim 2-3\ GM/c^2$), and becomes shallower as the radius increases. Then beyond $\sim 10\ GM/c^2$, it becomes steeper again. We fit the emissivity profile in different regions on the accretion disc with a power-law model (i.e., $\varepsilon(r) \propto r^{-q}$) using the least squared method, and summarize the results in Table 1. In the innermost region of the accretion disc ($r \leq 2\ GM/c^2$), the emissivity profile becomes steeper as the corona radius decreases. Far away from the black hole ($r \geq 20\ GM/c^2$), the indices are roughly consistent with the Newtonian value of 3.

Table 1. Measurements of emissivity and illumination indices for spherical coronae of different sizes

Corona radius $[GM/c^2]$	1	2	4	8
Emissivity profile				
$q\ (r \leq 2\ GM/c^2)$	6.55	6.49	6.32	5.67
$q\ (r \geq 20\ GM/c^2)$	2.97	3.00	2.98	3.02
Illumination profile				
$q\ (r \leq 2\ GM/c^2)$	2.92	2.92	2.96	3.27
$q\ (r \geq 20\ GM/c^2)$	3.06	3.06	3.07	3.09

The illumination profile has a similar three-segment broken power-law profile but in the innermost region it is shallower than the emissivity profile. We also fit the profiles with a power-law model and present the results in Table 1. We measure the photon index of the illuminating radiation in the energy band of 20–100 keV and find it to be ~ 3, greater than 2. According to Dovciak et al. (2014), in the innermost region of the accretion disc

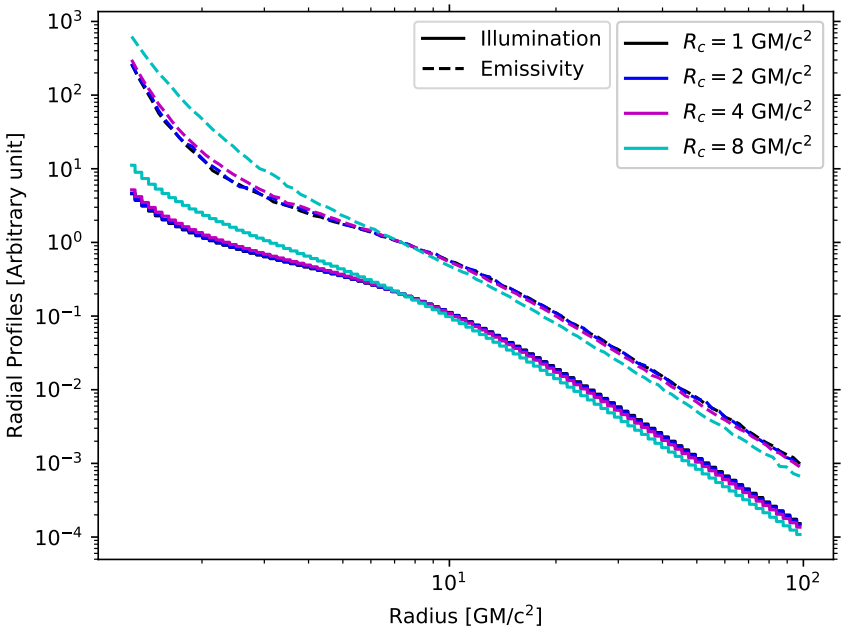

Figure 1. The illumination (solid lines) and emissivity (dashed lines) profiles of accretion discs illuminated by stationary spherical coronae of different sizes.

$g(r)$ increases with decreasing radius. Therefore the result that the emissivity profile is steeper than the illumination profile is consistent with the conclusion drawn in Sec. 2.2.

3.1.2 Dependence on corona height

In Fig. 2 we present the illumination and emissivity profiles for spherical coronae located at different heights above the equatorial plane. The radius of the coronae is 1 GM/c^2. We fit the emissivity and illumination profiles in different regions with a power-law model and summarise the results in Table 2. In the innermost region, as the height increases, the emissivity profile becomes steeper. The illumination profile is shallower than the emissivity profile.

3.2 Co-rotating slab corona in AGNs

In this section we present the results for accretion discs irradiated by slab coronae above the disc. The slab coronae are co-rotating with the underlying accretion disc. The thickness of the slab is 2 GM/c^2. The optical depth of the corona along the vertical direction is $\tau_T \equiv n_e \sigma_T h/2 = 0.2$, and the temperature of the corona is 100 keV. The black hole and thin disc have the same properties as in the previous subsection.

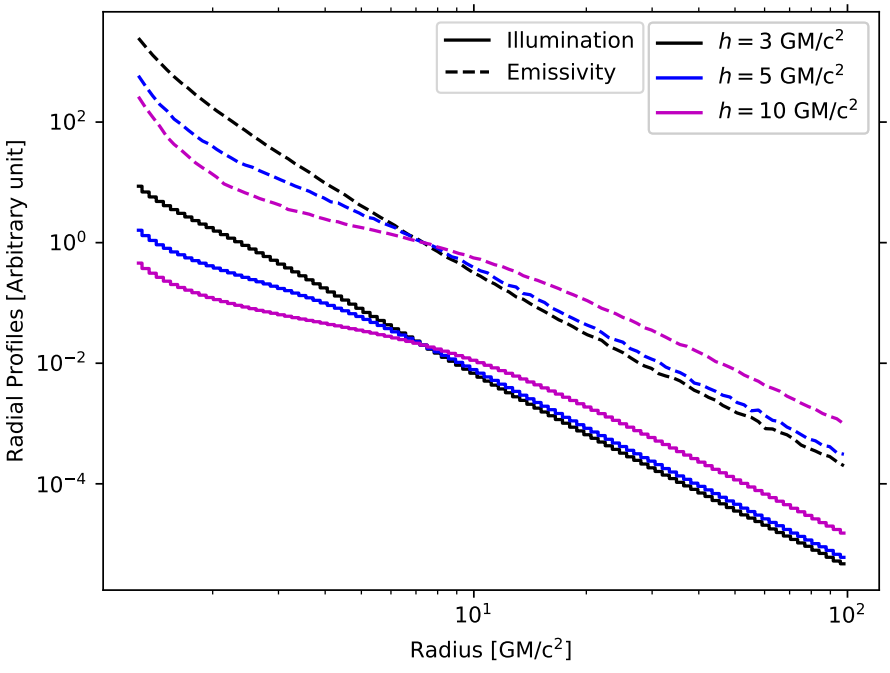

Figure 2. The illumination (solid lines) and emissivity (dashed lines) profiles of accretion discs illuminated by stationary spherical coronae located at different heights above the accretion disc.

Table 2. Measurements of emissivity and illumination indices for spherical coronae of different heights

Corona height $[GM/c^2]$	3	5	10
Emissivity profile			
$q\ (r \leq 2\ GM/c^2)$	5.80	5.90	6.55
$q\ (r \geq 20\ GM/c^2)$	3.15	3.13	2.97
Illumination profile			
$q\ (r \leq 2\ GM/c^2)$	3.52	3.01	2.92
$q\ (r \geq 20\ GM/c^2)$	3.13	3.12	3.06

3.2.1 Dependence on corona size

In Fig. 3 we present the illumination and emissivity profiles for accretion discs irradiated by slab coronae of different sizes. We measure the emissivity and illumination indices and

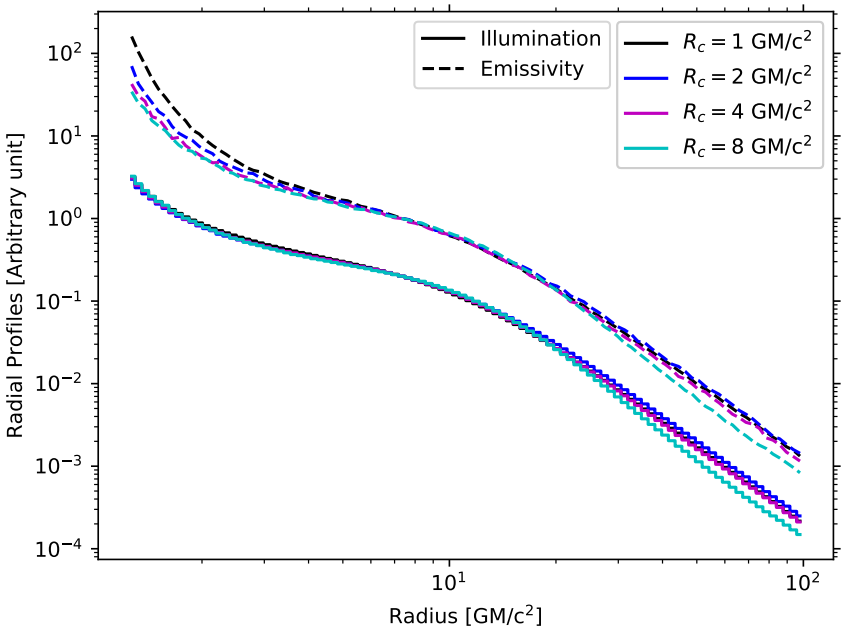

Figure 3. The illumination and emissivity profiles of accretion discs illuminated by co-rotating slab coronae of different sizes.

summarise the results in Table 3. Compared with the spherical coronae, the emissivity profile is more sensitive to the corona size, with shallower emissivity from more extended corona. Similarly with spherical coronae, the illumination profile is shallower than the emissivity profile given the same corona size.

Table 3. Measurements of emissivity and illumination indices for slab coronae of different sizes

Corona radius $[GM/c^2]$	1	2	4	8
Emissivity profile				
$q\ (r \leq 2\ GM/c^2)$	6.09	4.82	4.42	4.09
$q\ (r \geq 20\ GM/c^2)$	2.95	2.97	3.00	3.26
Illumination profile				
$q\ (r \leq 2\ GM/c^2)$	2.84	2.84	2.92	3.00
$q\ (r \geq 20\ GM/c^2)$	3.06	3.05	3.08	3.31

3.2.2 Dependence on corona height

In Fig. 4 we present the illumination and emissivity profiles for accretion discs irradiated by slab coronae located at different heights above the accretion disc. As the height increases, both the emissivity and the illumination profiles become steeper in the innermost region.

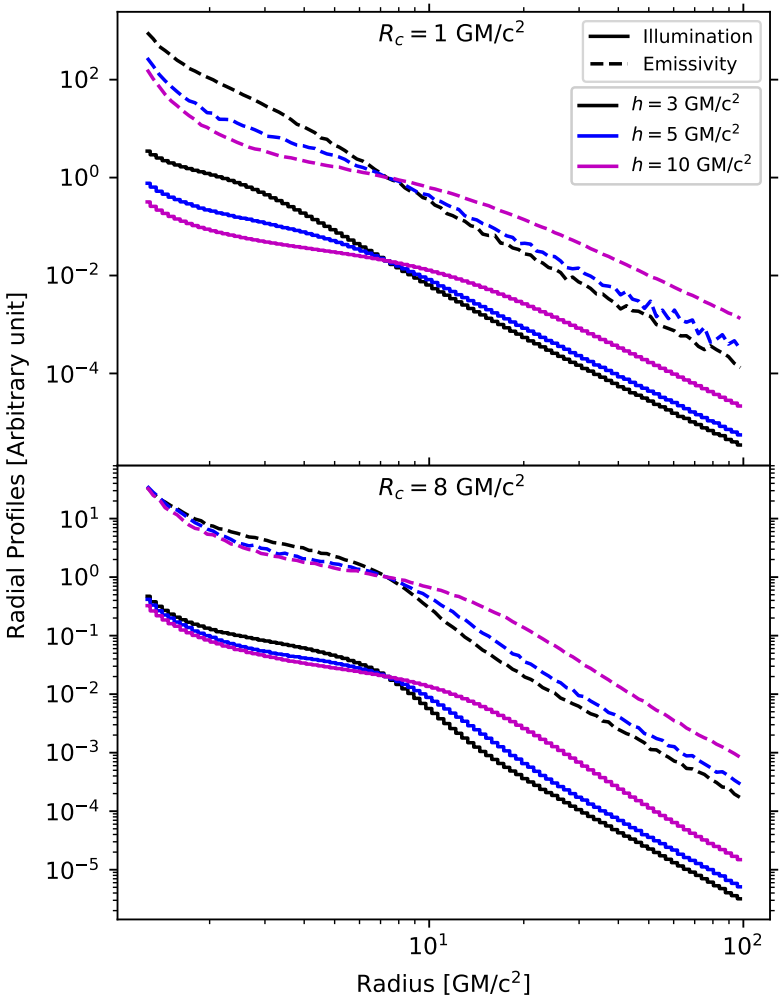

Figure 4. The illumination and emissivity profiles for accretion discs illuminated by co-rotating slab coronae located at different heights above the accretion discs. In the upper and lower panels we present the profiles for corona radii of 1 and 8 GM/c^2, respectively.

Table 4. Measurements of emissivity and illumination indices for slab coronae of different heights

Corona height $[GM/c^2]$	3	5	10
$R_c = 1\ GM/c^2$			
Emissivity profile			
$q\ (r \leq 2\ GM/c^2)$	4.72	5.60	6.09
$q\ (r \geq 20\ GM/c^2)$	3.28	3.11	2.95
Illumination profile			
$q\ (r \leq 2\ GM/c^2)$	2.30	2.78	2.84
$q\ (r \geq 20\ GM/c^2)$	3.19	3.17	3.06
$R_c = 8\ GM/c^2$			
Emissivity profile			
$q\ (r \leq 2\ GM/c^2)$	3.19	3.74	4.09
$q\ (r \geq 20\ GM/c^2)$	2.97	3.02	3.26
Illumination profile			
$q\ (r \leq 2\ GM/c^2)$	2.77	3.15	3.00
$q\ (r \geq 20\ GM/c^2)$	2.98	3.02	3.31

3.3 Stationary spherical coronae in XRBs

In the upper panel of Fig. 5 we present the illumination and emissivity profiles of accretion discs in XRBs illuminated by spherical coronae. The parameters are the same with Sec. 3.1, but for a $M = 10\ \mathrm{M}_\odot$ black hole accretion at a rate of 4.32×10^{17} g s^{-1} (corresponding to 10% Eddington luminosity). The emissivity profile is distinct compared with the emissivity profile of AGNs (Fig. 1) in that the profile is shallower than the Newtonian case below $\sim 10\ GM/c^2$, and the emissivity even decreases towards lower radius below $\sim 1.6\ GM/c^2$.

To highlight the distinction in the emissivity profile, in the lower panel of Fig. 5 we compare the profiles of accretion discs around 10 $\mathrm{M}_\odot$ and 10^7 $\mathrm{M}_\odot$ black holes. The illumination profiles are identical while the difference in the emissivity profile is obvious. To understand the difference, we calculate the spectra of the illuminating radiation as observed by the disc fluid at radii of 1.27, 1.58, and 2.67 GM/c^2, respectively, and present the results in Fig. 6. For $M = 10^7\ \mathrm{M}_\odot$, the low-energy cut-off is much lower than E_K, as a result a higher redshift simply leads to more X-ray photons above E_K; whereas for the 10 $\mathrm{M}_\odot$ case, the low-energy cut-off of the count spectra is in the range of 2 – 10 keV, resulting in a distinct emissivity profile. This indicates that the energy spectra of the hard X-ray radiation could substantially affect the emissivity profile.

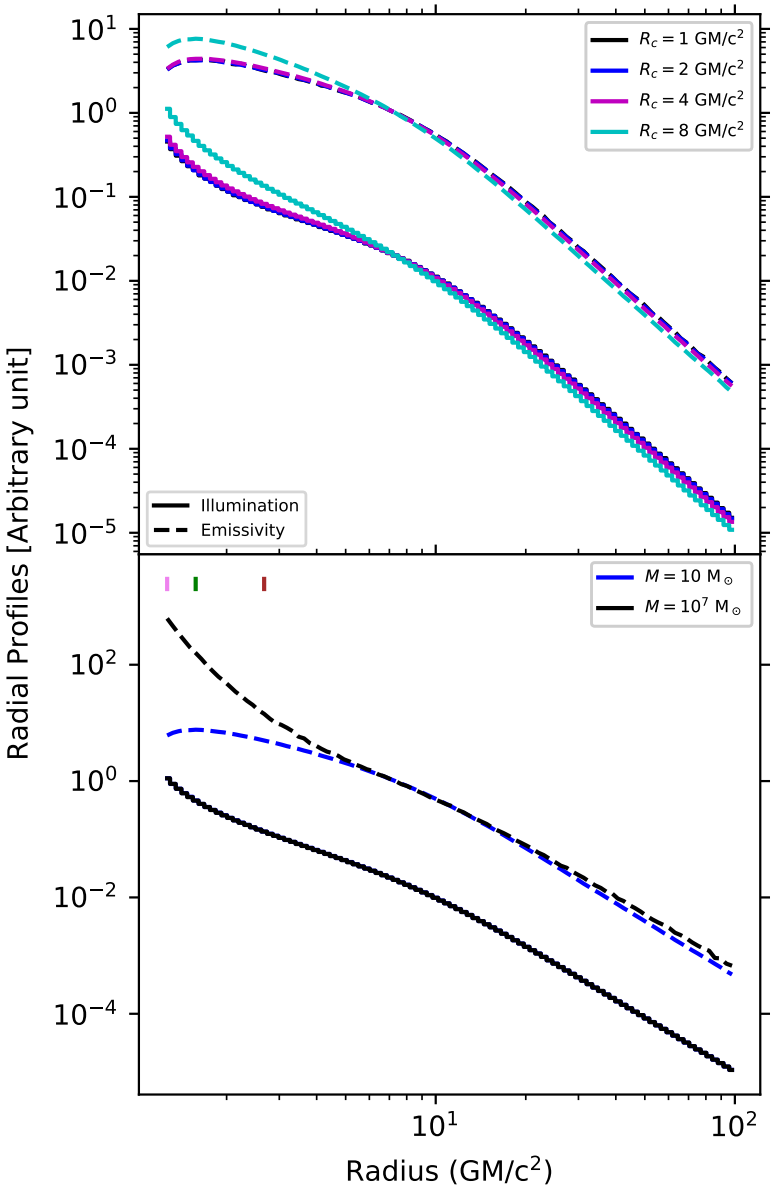

Figure 5. Upper panel: the illumination (dashed lines) and emissivity (solid lines) profiles of accretion discs illuminated by spherical coronae of different sizes. The accretion disc is rotating about a 10 $M_\odot$ black hole. Lower panel: comparison of the profiles between accretion discs around a 10 black hole (black) and a 10^7 $M_\odot$ black hole (blue). The violet, green, and brown vertical bars indicate the locations the spectra of which are plotted in Fig. 6.

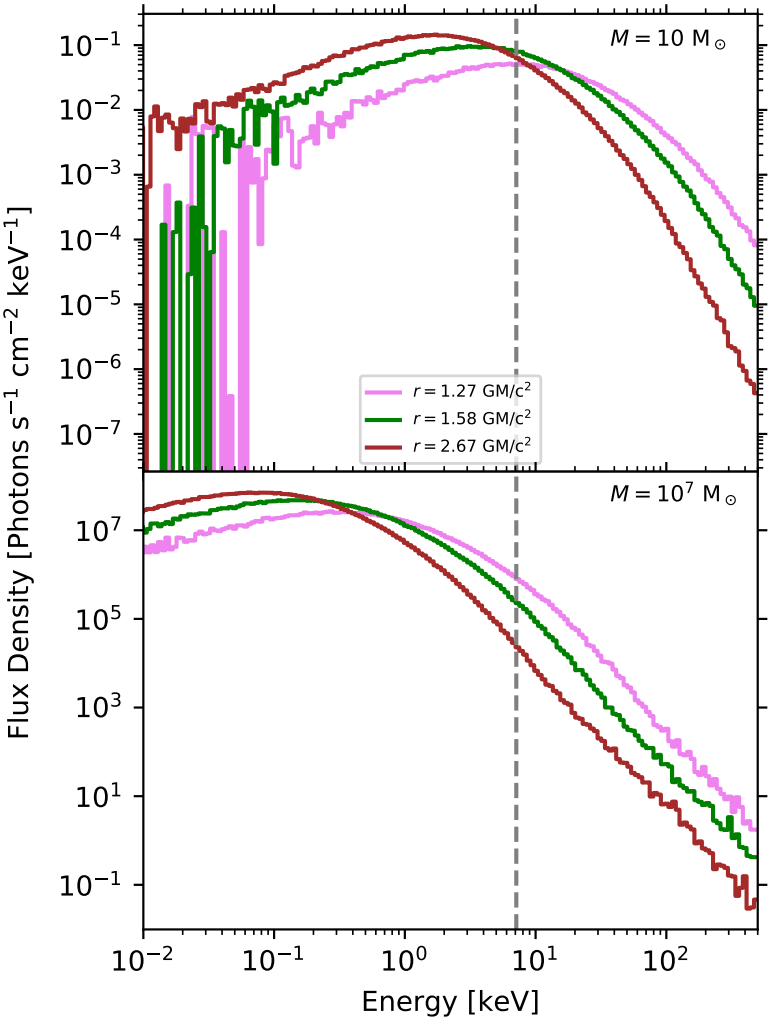

Figure 6. The energy spectra of the illuminating radiation observed by disc fluid located at different radii. The spherical corona is located 10 GM/c^2 above the accretion disc and has radius of 1 GM/c^2. The spectra at different radii are plotted in different colors, while the locations are indicated by the vertical bars in Fig. 5. The vertical dashed line indicates the location of neutral iron K edge at 7.12 keV. In the upper and lower panels we present the spectra for accretion discs around 10 and 10^7 $M_\odot$, respectively.

4 SUMMARY

In this work we present the illumination and neutral iron Kα emissivity profiles of accretion discs irradiated by extended coronae. With our GR Monte Carlo radiative transfer code Monk, we can calculate the energy spectrum of the illuminating radiation in the rest frame of the accretion disc. As a result, we are able to calculate both the illumination and emissivity profiles while in most previous studies the authors did not make a clear distinction between the two. For AGN discs, the emissivity profiles are in general steeper than the illumination profiles for the parameters taken in the calculations; whereas for accretion discs in black hole X-ray binaries, the distinction is more dramatic: the emissivity even decreases with decreasing radius in the innermost region of the disc. We find out that the different behaviors in AGNs and black hole X-ray binaries are due to the difference in energy spectra of the illuminating radiation as seen by the disc. This suggests that the emissivity profile of the iron Kα line cannot be determined by black hole spin and corona geometry alone, and the energy spectrum of the illuminating radiation has to be taken into account. We also study the dependence of the emissivity profile on the geometry of the corona and find the emissivity in the innermost region of the disc steepens as the corona becomes less extended or as the corona has a larger height.

ACKNOWLEDGEMENTS

The authors acknowledge financial support provided by Czech Science Foundation grant 17-02430S. This work is also supported by the project RVO:67985815. This research makes uses of Matplotlib (Hunter, 2007), a Python 2D plotting library which produces publication quality figures.

REFERENCES

Dolence, J. C., Gammie, C. F., Mościbrodzka, M. and Leung, P. K. (2009), Grmonty: A Monte Carlo Code for Relativistic Radiative Transport, *ApJS*, **184**, pp. 387–397, ISSN 0067-0049.

Dovciak, M., Svoboda, J., Goosmann, R. W., Karas, V., Matt, G. and Sochora, V. (2014), An XSPEC model to explore spectral features from black-hole sources - II. The relativistic iron line in the lamp-post geometry, *arXiv:1412.8627*, arXiv: 1412.8627.

Eckart, A., Schödel, R., Meyer, L., Trippe, S., Ott, T. and Genzel, R. (2006), Polarimetry of near-infrared flares from Sagittarius A*, *A&A*, **455**, pp. 1–10, ISSN 0004-6361.

Fabian, A. C., Rees, M. J., Stella, L. and White, N. E. (1989), X-ray fluorescence from the inner disc in Cygnus X-1, *MNRAS*, **238**, pp. 729–736, ISSN 0035-8711.

Fabian, A. C. and Ross, R. R. (2010), X-ray Reflection, *Space Science Reviews*, **157**, pp. 167–176, ISSN 0038-6308.

George, I. M. and Fabian, A. C. (1991), X-ray reflection from cold matter in active galactic nuclei and X-ray binaries, *MNRAS*, **249**, pp. 352–367, ISSN 0035-8711.

Gonzalez, A. G., Wilkins, D. R. and Gallo, L. C. (2017), Probing the geometry and motion of AGN coronae through accretion disc emissivity profiles, *MNRAS*, **472**, pp. 1932–1945, ISSN 0035-8711.

Grevesse, N. and Sauval, A. J. (1998), Standard Solar Composition, *Space Science Reviews*, **85**, pp. 161–174, ISSN 0038-6308.

Hunter, J. D. (2007), Matplotlib: A 2D Graphics Environment, *Computing In Science Engineering*, **9**(3), pp. 90–95, ISSN 1521-9615.

Karssen, G. D., Bursa, M., Eckart, A., Valencia-S, M., Dovčiak, M., Karas, V. and Horák, J. (2017), Bright X-ray flares from Sgr A*, *MNRAS*, **472**, pp. 4422–4433, ISSN 0035-8711.

Laor, A. (1991), Line profiles from a disk around a rotating black hole, *ApJ*, **376**, pp. 90–94, ISSN 0004-637X.

Lusso, E., Comastri, A., Simmons, B. D., Mignoli, M., Zamorani, G., Vignali, C., Brusa, M., Shankar, F., Lutz, D., Trump, J. R., Maiolino, R., Gilli, R., Bolzonella, M., Puccetti, S., Salvato, M., Impey, C. D., Civano, F., Elvis, M., Mainieri, V., Silverman, J. D., Koekemoer, A. M., Bongiorno, A., Merloni, A., Berta, S., Le Floc'h, E., Magnelli, B., Pozzi, F. and Riguccini, L. (2012), Bolometric luminosities and Eddington ratios of X-ray selected active galactic nuclei in the XMM-COSMOS survey, *MNRAS*, **425**, pp. 623–640, ISSN 0035-8711.

Martocchia, A., Karas, V. and Matt, G. (2000), Effects of Kerr space-time on spectral features from X-ray illuminated accretion discs, *MNRAS*, **312**, pp. 817–826, ISSN 0035-8711.

Miller, J. M. (2007), Relativistic X-Ray Lines from the Inner Accretion Disks Around Black Holes, *Annual Review Of Astronomy Astrophysics*, **45**, pp. 441–479, ISSN 0066-4146.

Miller, J. M., Reynolds, C. S., Fabian, A. C., Miniutti, G. and Gallo, L. C. (2009), Stellar-Mass Black Hole Spin Constraints from Disk Reflection and Continuum Modeling, *ApJ*, **697**, pp. 900–912, ISSN 0004-637X.

Miniutti, G., Fabian, A. C., Goyder, R. and Lasenby, A. N. (2003), The lack of variability of the iron line in MCG-6-30-15: General relativistic effects, *MNRAS*, **344**, pp. L22–L26, ISSN 0035-8711.

Shcherbakov, R. V., Penna, R. F. and McKinney, J. C. (2012), Sagittarius A* Accretion Flow and Black Hole Parameters from General Relativistic Dynamical and Polarized Radiative Modeling, *ApJ*, **755**, p. 133, ISSN 0004-637X.

Trippe, S., Paumard, T., Ott, T., Gillessen, S., Eisenhauer, F., Martins, F. and Genzel, R. (2007), A polarized infrared flare from Sagittarius A* and the signatures of orbiting plasma hotspots, *MNRAS*, **375**, pp. 764–772, ISSN 0035-8711.

Verner, D. A. and Yakovlev, D. G. (1995), Analytic FITS for partial photoionization cross sections., *Astronomy Astrophysics Supplement Series*, **109**, pp. 125–133, ISSN 0365-0138.

Wilkins, D. R. and Fabian, A. C. (2012), Understanding X-ray reflection emissivity profiles in AGN: Locating the X-ray source, *MNRAS*, **424**, pp. 1284–1296, ISSN 0035-8711.

Zhang, W., Dovčiak, M. and Bursa, M. (2019), Constraining the Size of the Corona with Fully Relativistic Calculations of Spectra of Extended Coronae. I. The Monte Carlo Radiative Transfer Code, *ApJ*, **875**(2), p. 148.